JMEPEG (2007) 16:607–613
DOI: 10.1007/s11665-007-9065-8

1059-9495/$19.00

Fracture Properties and Fracture Surface Morphologies in Rubber-PMMA Composites

Shiyun Gong and Sri Bandyopadhyay

(Submitted April 13, 2006)

Correlations between fracture properties and microscopic features were investigated using notched (both blunt notched and sharp notched) specimens of rubber-PMMA composites in very low-to-medium range of cross-head speeds. It is found that: (1) the decreasing trend of crack initiation region size with increasing speed correlates with the fracture elongation; (2) the decreasing trend of SWZ size with increasing speed and decreasing rubber content can be correlated with that of calculated plastic zone and the trend correlates also with that in modulus of toughness; (3) the order of degree of material plastic flow at notch tip in the polymers correlates with the corresponding order of their *K* values.

Keywords electron microscopy, fractography, fracture toughness, mechanical properties, PMMA and blends

1. Introduction

Toughened polymers, in the form of copolymers or blends, are very important materials consisting of a high-modulus phase with modulus of elasticity (E) typically 3 GPa, and a low-modulus rubbery phase with E of the order of a few to several MPa. The deformation mechanisms of toughened polymers have been extensively studied in the literature but not yet properly understood because the base thermoplastic or thermoset polymers can undergo plastic deformation by mixed modes of shear yielding and crazing (Ref 1-3). The addition of the soft phase can add/induce more complexity in the deformation behavior of toughened polymers either as an inclusion, an interface or interphase, raiser of triaxiality, a bridge-forming element or by its own deformation modality. Examples of conventional unnotched testing as a function of strain rate and temperature (Ref 4-6) as well as fracture mechanics-based notched specimen testing under pseudostatic and impact rates (Ref 7) are available in the literature. In recent work, ductile-brittle transition and dynamic fracture studies have been employed in toughened glassy polymers (Ref 8-10), whereas micromechanical studies and ultrasonic measurements undertaken in toughened glassy polymers, semicrystalline polymers, or polymer matrix composites (Ref 11-13) have yielded useful information. In addition, more recent studies concerning crack velocity and corresponding fracture surfaces (Ref 14-16), stress concentration at notch tip (Ref 17), and morphologies in different part of the fracture surface (Ref 18) give us a good understanding of deformation and fracture mechanisms.

However, some aspects or problems in the field have not been explored adequately and systematically. Here are some examples. It is known that toughened plastics are viscoelastic in nature (Ref 19-22), and test speed has a significant effect on test results; however, medium-to-high test speeds have generally been employed in the literature mostly because these tests are less time-consuming (hence less expensive) and this has left a significant gap in data in the lower range of test speeds. Second, it is known that a notch can markedly reduce fracture stress of a brittle glassy polymer like poly(methyl methacrylate) (PMMA) and make ductile materials like rubber-toughened PMMA (RTPMMA) fail in a brittle manner (Ref 23); however, it is little-known how the difference in the fracture surface morphologies for the two modes of fracture looks like.

The present authors take the view that study of toughened polymers should be investigated from a broader point of view. This means not only that both conventional unnotched and fracture mechanics-based notched tests need to be carried out experimentally on the same materials under identical test conditions to get comparative and meaningful results, but also that extensive scanning and transmission electron microscopic studies need to be carried out systematically in later stage to obtain correlations between macroscopic mechanical properties and microscopic features on the fracture surfaces of test specimens to identify and support/complement the findings of the mechanical test results and get a global understanding of the findings.

This research studies commercial grades of toughened polymers as these are the ones available in the open market for use in actual engineering applications. Moreover, the research employs slow-to-medium test speeds to fill a significant gap in data in the lower range of test speeds. Particularly, the research devotes attention to the microscopic examination of deformation/fracture features, in an attempt to reveal correlations between macroscopic properties and microscopic features.

Part I of this work using unnotched specimens has been submitted (Ref 24). This article, part II presents the results

Shiyun Gong, College of Materials Science and Engineering, Harbin University of Science and Technology, Harbin 150040, China. Contact e-mail: shiyun@yahoo.com; and **Sri Bandyopadhyay,** School of Materials Science and Engineering, University of New South Wales, Sydney 2052, Australia.

using only the notched specimens (both blunt notched and sharp notched).

2. Experimental

2.1 Materials

Main test materials selected for the program are two commercial grades of RTPMMA from Cadillac Plastics Sydney, Australia—5× PMMA and 8× PMMA significantly differing in rubber content, termed as RTPMMA-1 and RTPMMA-2, respectively. An untoughened (pure) PMMA obtained from the same commercial source is also studied in parallel as a control material against which RTPMMA-1 and RTPMMA-2 are compared. The cast sheets of the three materials were purchased from Cadillac Plastics Sydney, Australia; however, the materials information was not released. Therefore, we determined experimentally on our own the materials information such as rubber particle structure and rubber content, using characterization methods such as transmission electron microscopy (TEM) examination and calculations based on the rule of mixtures (Ref 25). Details of the materials are given in Table 1.

2.2 Experimental program

Single-edge notch (SEN) of depth 3 mm and notch root radius of 0.30 mm was machine-cut in the middle of the length of each of the tensile test specimens (similar to ASTM D 256 Charpy type specimens), which forms the blunt notched specimen. Sharp notched specimens were made by sliding a razor blade at the tip of the blunt notch. The shape and key dimensions were in accordance with ASTM D 638 and D 256. Three specimens for each material were tested at each speed.

The tests were conducted, on both blunt and sharp notched specimens, in an Instron Model 1185 Testing Machine, at cross-head speeds (CHS): 0.05, 0.5, 1, 5, and 10 mm/min. Logarithmic values of CHSs and their corresponding strain rates are given in Table 2, where strain rate is obtained by dividing CHS by gauge length, i.e., 50 mm and then changing to s^{-1}.

The load and the cross-head displacement were recorded on a strip chart recorder. Cross head and chart speeds were set at 1:1. The full scale load was set at 5 kN for PMMA, and 2 kN for RTPMMA-1 and RTPMMA-2.

Stress intensity factor values for blunt notches (K_b) and sharp notches (K_{IC}) can be calculated using the equation (Ref 23)

$$K_I = Pa^{1/2}\left[1.99 - 0.41\left(\frac{a}{W}\right) + 18.70\left(\frac{a}{W}\right)^2 - 38.48\left(\frac{a}{W}\right)^3 + 53.85\left(\frac{a}{W}\right)^4\right] \Big/ BW, \quad \text{(Eq 1)}$$

where P is maximum load on the load-deflection curve; B specimen thickness; W specimen width; a initial crack length (for a sharp notched specimen, it is equal to the depth of machined notch plus the depth of razor notch, measured using a traveling microscope). Fracture surfaces from the tensile tests were flat and square, i.e., apparently in plane strain condition. Thus, we can use the equation for the calculation of K_b and K_{IC}.

The radius of plastic zone r_p (or Dugdale's analysis δa) as well as the critical crack length $\bar{a}$ for RTPMMA can be worked out, using the relationship

$$r_p = K_C^2/2\pi\sigma_y^2 = \bar{a}/2 = 4\delta a/\pi^2, \quad \text{(Eq 2)}$$

where σ_y is yield stress.

Specimens for scanning electron microscopy (SEM) and field emission SEM (FESEM) examinations of fracture surface were saw-cut from the fractured test specimens, about 5 mm below fracture surface, which were mounted on aluminum stubs (∅25 × 5 mm) after cleaning, and then coated with gold in a JEOL JEE-400 Vacuum Evaporator.

Scanning electron microscopy examination of gold-coated fracture surfaces were performed in a JEOL LXA-840 Scanning Microanalyzer for low magnifications (lower than 3000), and FESEM examination a HITACHI S-4500 Scanning Electron Microscope for high magnifications (5000× or 10,000×). To prevent fracture surface from being damaged during examination, low accelerating voltages were used. The satisfactory result was obtained by using accelerating voltages of 5 kV for SEM and 1 kV for FESEM.

Table 1 Test materials and their physical characteristics

Testing material and nature	Thickness of sheet, mm	Rubber particle structure, from TEM exam.	Content of rubber particles, vol.%, from TEM exam.	Content of rubber, vol.%, from rule of mixtures	T_g, glass trans temp., from DSC test, °C
Pure PMMA, transparent	4	Not applicable	0	0	117
5× RTPMMA (RTPMMA-1), transparent, five times more ductile than pure PMMA	3	Hard core-soft shell (three layer particles)	17.8	13.8	111
8× RTPMMA (RTPMMA-2), transparent, eight times more ductile than pure PMMA	3	Hard core-soft shell (three layer particles)	41.9	41.4	110

Table 2 Logarithmic values of CHSs and their corresponding strain rates

CHS, mm/min	0.05	0.5	1	5	10
lnCHS	−3	−0.69	0	1.61	2.30
$\dot{e}$, s^{-1}	1.67×10^{-5}	1.67×10^{-4}	3.33×10^{-4}	1.67×10^{-3}	3.33×10^{-3}
ln $\dot{e}$	−11	−8.7	−8	−6.4	−5.7

3. Results and Discussion

3.1 Fracture Properties

The values of fracture stress for notched specimens are presented in Table 3. Based on the data, K_{IC} and K_b in $MPam^{1/2}$ were worked out, using the SEN calibration equation (1), and are plotted graphically as a function of lnCHS in Fig. 1(a) and (b), respectively.

It is seen in Fig. 1 that: (1) with rubber toughening, K_{IC} value of PMMA is increased by a factor of 2; (2) blunt notch or sharp crack does not really make a big difference in the K_{IC} or K_b values for the materials; (3) RTPMMA-2 containing much more rubber has apparently a lower K_{IC} value than RTPMMA-1. This indicates that either: (a) there is an optimum amount of rubber for incorporation, which can improve the material's maximum ability of resistance to crack best, or (b) more plausibly, lowering of the modulus lowers the K_{IC} value through the equation $K^2 = EG_{IC}$, where G_{IC} is fracture energy, although more rubber would result in a higher G_{IC}; (4) a slight decrease in K value with increasing CHS for RTPMMA indicates a restricted plastic flow (global yield) at notch tip. Details of the material plastic flow at notch tip will be presented in the following part.

It is also noticed that the K_{IC} values for the PMMA and RTPMMA-1 agree with those for the pure PMMA and RTPMMA materials (1.22 and 2.8 $MPam^{1/2}$, respectively) obtained by Lovell et al. (Ref 26).

With the available values of K_{IC} and yield stress σ_y, the radius of plastic zone r_p (or Dugdale's analysis δa) as well as the critical crack length $\bar{a}$ for RTPMMA can be worked out, using Eq 2. From the calculation results given in Table 4, following points can be drawn: (1) the plastic zone at higher speed is much smaller than that at lower speed, and critical crack length has a similar trend; (2) RTPMMA-2 has greater values of both r_p (or δa) and $\bar{a}$ than RTPMMA-1. It will be shown in next part that $\bar{a}$ values in Table 4 are very closer to the values of measured stress whitening zone (SWZ), indicating that the SWZ actually represents the subcritical (slow) crack growth. Once the crack reaches this value, instability sets in.

3.2 Fracture Surface Morphologies and Correlations with Fracture Properties

Photographs of fracture surfaces in both blunt and sharp notched PMMA polymers at both low and high magnifications are presented here and surface features are discussed to reach correlations.

3.2.1 Surface Features at Low Magnifications. Low magnification (12×) SEM fracture surfaces in pure PMMA at two extreme ends of the CHS range, i.e., 0.05 and 10 mm/min

Table 3 Average values of fracture stress in MPa for notched specimens

Material		CHS, mm/min				
		0.05	0.5	1.0	5.0	10.0
PMMA	Blunt	8.7	8.9	10.0	10.8	10.2
	Sharp	8.1	8.4	8.7	9.4	9.3
RTPMMA-1	Blunt	22.5	21.1	20.9	19.5	19.4
	Sharp	18.1	16.4	16.5	16.4	17.1
RTPMMA-2	Blunt	17.9	19.1	19.2	19.5	20.1
	Sharp	15.6	15.8	14.6	14.0	12.2

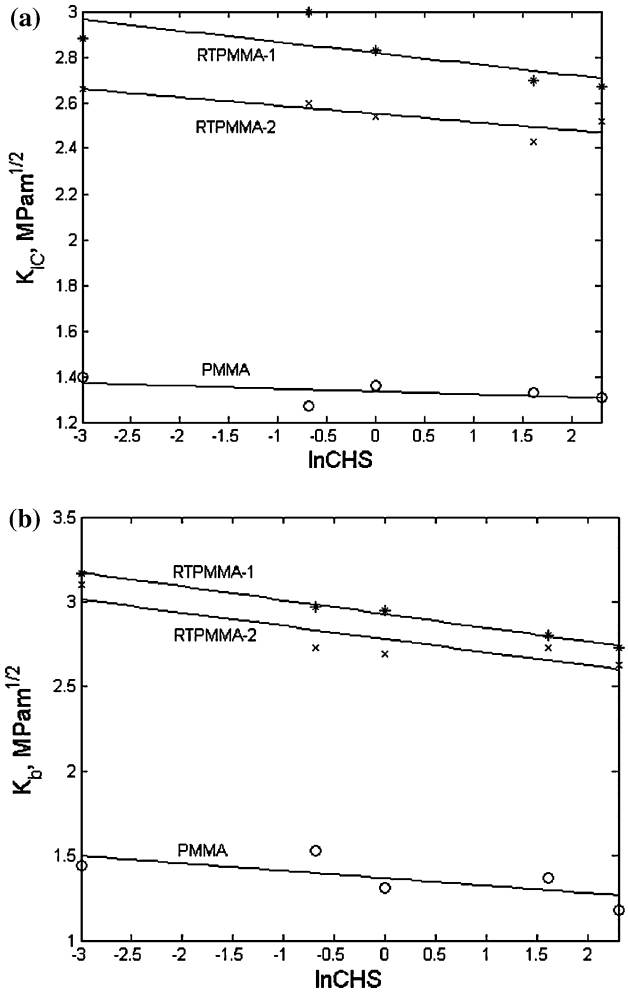

Fig. 1 K_{IC} and K_b vs. natural logarithm of cross-head speed; (a) K_{IC}, (b) K_b

are shown in Fig. 2, and low magnification (6×) optical fracture surfaces with SWZ in RTPMMA at CHSs 0.05, 0.5, 1, 5, and 10 mm/min are presented in Fig. 3. Figure 4 illustrates main features of the fracture surfaces in the three notched materials.

It is seen that the whole fracture surface in notched PMMA is smooth like a glass surface in daily life, which is totally different from that of unnotched one in paper I (Ref 24). An arrest line divides the surface into two regions (1 and 2), and interference color fringes were frequently observed in the crack initiation region (region 1). In addition, size of the crack initiation region is rate-dependent; the decreasing trend of the initiation region size with increasing speed correlates with the fracture elongation as discussed in paper I (Ref 24).

Obviously different from notched PMMA, notched RTPMMA-1 has two totally different regions as shown schematically in Fig. 4(b): a rough region with 'violent' form of crack propagation and a smooth region with SWZ of ductile crack initiation starting at notch tip; by contrast, the fracture surface in notched RTPMMA-2 bears no arrest line and no rough region, which can be regarded as a single smooth region with SWZ starting at notch tip.

It is also noted in Fig. 3(a) and (b) that a fine white line lies in smooth region in notched RTPMMA-1 just before transition. Width of the white line and distance from the line to transition

Table 4 Calculated values of r_p, δa and $\bar{a}$ at CHS 0.05 and 10 mm/min for RTPMMA

	RTPMMA-1		RTPMMA-2	
Item	**0.05**	**10**	**0.05**	**10**
$r_{p,}$ mm	0.70	0.30	1.15	0.50
$\bar{a}$, mm	1.40	0.60	2.30	1.00
δa, mm	1.73	0.74	2.83	1.23

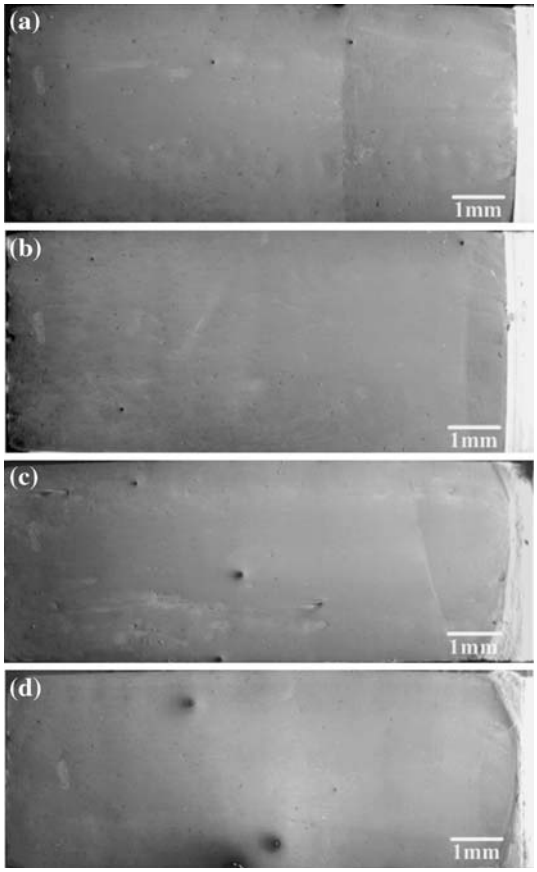

Fig. 2 Low magnification (12×) SEM fracture surfaces in notched PMMA (notch at the right, i.e., crack propagating from right to left). (a) Blunt notched PMMA at CHS 0.05 mm/min, (b) blunt notched PMMA at CHS 10 mm/min, (c) sharp notched PMMA at CHS 0.05 mm/min, (d) sharp notched PMMA at CHS 10 mm/min

line as well as distance form notch tip to transition line, i.e., length of smooth region were measured. The white line is about 0.05 mm in width, lying just about 0.25 mm before transition line for blunt notched RTPMMA-1 and about 0.30 mm before transition line for sharp notched RTPMMA-1; length from notch tip to transition line, i.e., length of smooth region does not seem to be changed much with increasing CHS among specimens; however, it does differ between different notch states, i.e., the sharp notched is larger in smooth region (3.20 mm) than the blunt notched (2.40 mm). This detailed picture really reflects fluctuation of the crack velocity in smooth region and complexity of stress state at notch tip.

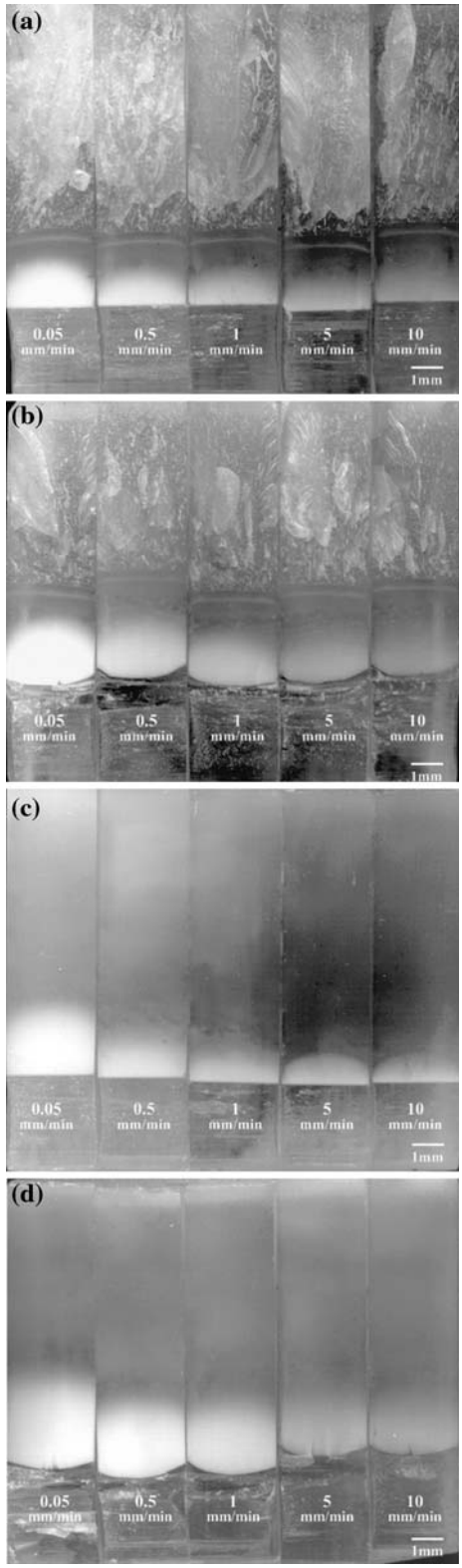

Fig. 3 SWZ and other features seen in low magnification (6×) optical photographs of notched RTPMMA at various CHSs (specimen at the lowest CHS, i.e., 0.05 mm/min arranged at the left most; notch at the bottom, i.e., crack propagating from bottom to top of the page). (a) Blunt notched RTPMMA-1, (b) sharp notched RTPMMA-1, (c) blunt notched RTPMMA-2, (d) sharp notched RTPMMA-2

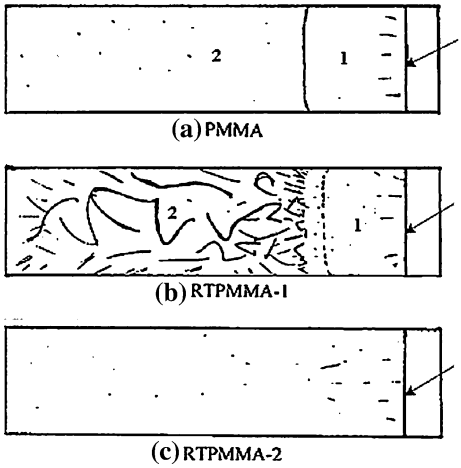

Fig. 4 Schematic representation of main features on low-magnification fracture surfaces in notched PMMA and RTPMMA (1—initiation region, i.e., slow, subcritical growth; 2—rough or fast crack propagation region; arrows pointing notch tip or fracture origin)

Among other features, the existence of SWZ starting at notch tip in smooth region is characteristic of RTPMMA. SWZ, as shown in Fig. 3 decreases in both size (length) and whiteness intensity as speed increases. Whitening appears to vary from milk at lower CHS to light haze at higher CHS, in terms of groups of five specimens, and vary gradually from milk closest at notch tip to light haze furthest away from notch tip on an individual surface and finally disappear. In general, no sharp ending of SWZ on an individual surface can be seen in Fig. 3.

Length of SWZ in fractured RTPMMA specimens was measured and the length data are plotted as a function of lnCHS in Fig. 5. It is seen that SWZ is influenced by speed, rubber content, and notch state. Specifically, (a) length of SWZ has a decreasing trend with increasing speed; (b) length of SWZ in notched RTPMMA-2 is larger than that in notched RTPMMA-1, indicating that more rubber favors greater SWZ; (c) length of SWZ in sharp notched specimens is larger than that in blunt notched ones, plausibly because the stress concentration at sharp notch tip is much higher than that at blunt notch tip.

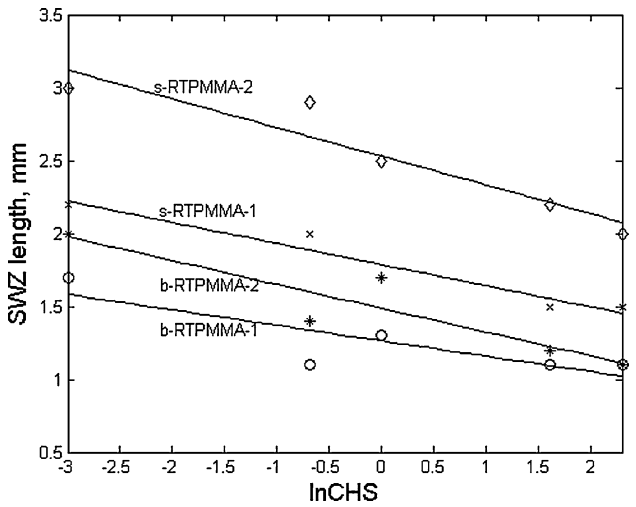

Fig. 5 SWZ variation with lnCHS (b, blunt notched; s, sharp notched)

In summary, the decreasing trend of SWZ size with increasing speed and decreasing rubber content can be correlated with that of calculated plastic zone; the trend correlates also with that in modulus of toughness as discussed in paper I (Ref 24). In addition, the SWZ actually represents the slow crack growth.

3.2.2 Surface Features at High Magnifications. The plastic deformation or material plastic flow near notch tip in the three investigated materials, and whitening mechanism in the RTPMMA are suggested by FESEM micrographs in Fig. 6 revealing the morphology near notch tip, and Fig. 7 revealing the morphology further away from notch tip.

Comparing the high magnification FESEM fracture surfaces in Fig. 6, one can see that (1) the surface in the vicinity of notch tip in RTPMMA exhibits dimples and/or voids which indicate the existence of rubber particles, while the surface in pure PMMA not; (2) more severe plastic deformation occurs in the vicinity of blunt notched tip, in terms of the weight of oriented tear lines and the number of voids/dimples, indicating that there is a significant difference in stress state (or even crack velocity) in the vicinity of notch tip between the blunt notched and sharp notched specimens.

Further, comparing the surfaces in RTPMMA-1 with ones in RTPMMA-2 in Fig. 6, one can also see that the toughened material containing more rubber, i.e., RTPMMA-2 is less plastically deformed at notch tip. In fact, degree of material plastic flow at notch tip seen in Fig. 6 is roughly of the order: $c > d \approx e > f > a > b$, i.e., blunt notched RTPMMA-1 > sharp notched RTPMMA-1 ≈ blunt notched RTPMMA-2 > sharp notched RTPMMA-2 > blunt notched PMMA > sharp notched PMMA, which correlates with the corresponding order of their K values in foregoing part. Therefore, it might be concluded that K parameter might not reflect how fast the crack can grow in initiation region in the material, i.e., it might not reflect other mechanisms accompanying crack evolution and causing localized yielding which were other factors determining actual fracture toughness in RTPMMA, although it reflect degree of material plastic flow at notch tip when the crack initiate which is influenced by both flow capacity of material itself and notch state. A good example for this is that RTPMMA-2 has lower K value than RTPMMA-1 but it has higher value in both fracture elongation and modulus of toughness than RTPMMA-1. It is strange to think a material with lower K value can absorb more energy during tension. Therefore, the K parameter might reflect only one side of the problem of fracture toughness.

In addition, as shown schematically in Fig. 4, both the fracture surface in notched PMMA and the fracture surface in notched RTPMMA-2 appear flat (no crack branching); however, at high magnifications, a difference is revealed: crack initiation region in notched RTPMMA-2 as shown in Fig. 6(e) and (f) is full of voids, while the one in notched PMMA in Fig. 6(a) and (b) not. The comparison suggests that it is those voids that scatter light and cause whitening, and formation process of those voids/dimples as well as fibrils absorbs energy which cause higher value in modulus of toughness in RTPMMA-2 as discussed in paper I (Ref 24).

Finally, Fig. 7 shows the morphology further away from SWZ in a sharp notched specimen of RTPMMA-1 whose morphology at notch tip is shown in Fig. 6(d). By comparing Fig. 7 with Fig. 6(d), it is further understood that it is those voids of over certain sizes that scatter light and cause

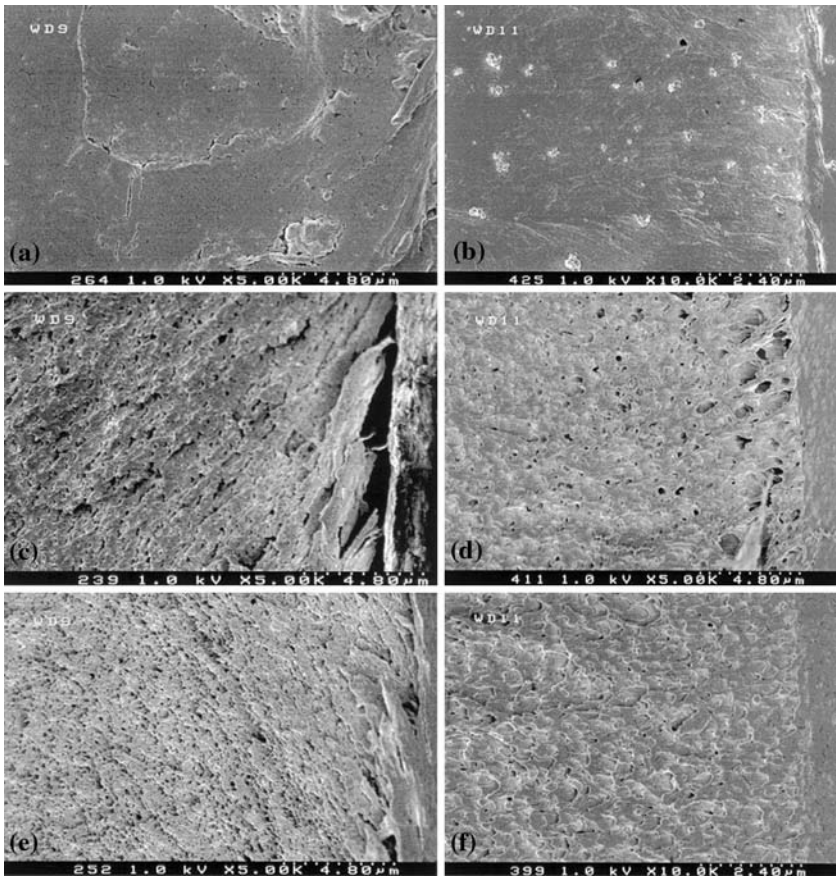

Fig. 6 FESEM micrographs showing plastic deformation in the vicinity of notch tip in the three notched polymers (a and b correspond to the specimens shown in Fig. 2(a) and (c), respectively; c, d, e, and f the specimens in Fig. 3(a)-(d) at CHS 0.05 mm/min, respectively; notch tip at right, i.e., crack propagating from right to left). (a) Blunt notched PMMA: inclined tear lines angled at about 60° to fracture direction; fine cracks were from gold coatings, (b) sharp notched PMMA: forward light tear lines, (c) blunt notched RTPMMA-1: heavily inclined tear lines angled at about 60° to fracture direction, and a large number of voids, (d) sharp notched RTPMMA-1: less heavily inclined tear lines, voids, and a large number of dimples, (e) blunt notched RTPMMA-2: heavily inclined tear lines angled at about 60° to fracture direction, voids, and fibrils, (f) sharp notched RTPMMA-2: voids, and tear dimples (Ref 27)

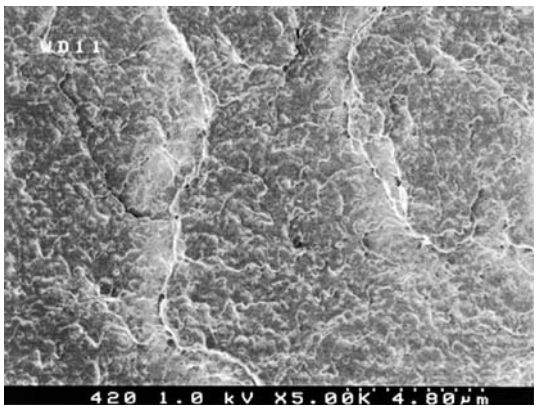

Fig. 7 FESEM micrograph showing morphology further away from SWZ in sharp notched RTPMMA-1 at CHS 0.05 mm/min presented in Fig. 3(b)

whitening. Moreover, it is observed in Fig. 6(d) that both number and general size of the voids become small, away from notch tip along crack acceleration path, which might be responsible for decrease in both size of SWZ and whiteness intensity with increasing distance from notch tip as well as increasing CHS.

4. Conclusions

(1) Size of crack initiation region in notched PMMA is rate-dependent. The decreasing trend of the initiation region size with increasing speed correlates with that of the fracture elongation.
(2) Size of SWZ in crack initiation region in notched RTPMMA is both rate-dependent and rubber content-dependent. The decreasing trend of SWZ size with increasing speed and decreasing rubber content can be correlated with that of calculated plastic zone. The trend correlates also with that in modulus of toughness.
(3) More severe plastic deformation occurs in the vicinity of blunt notched tip of the three investigated materials, in terms of the weight of oriented tear lines and the number of voids/dimples.
(4) Degree of material plastic flow at notch tip is roughly of the order: blunt notched RTPMMA-1 > sharp notched RTPMMA-1 ≈ blunt notched RTPMMA-2 > sharp

notched RTPMMA-2 > blunt notched PMMA > sharp notched PMMA, which correlates with the corresponding order of their K values.

(5) Toughness parameter K might not reflect other deformation processes which can occur in RTPMMA during tension and absorb energy, although it reflect material plastic flow at notch tip.

References

1. C.B. Bucknall, *Toughened Plastics*. Applied Science Publishers Ltd, London, 1977
2. I.M. Ward, *Mechanical Properties of Solid Polymers*. 2nd ed., John Wiley & Sons Ltd, New York, 1990
3. S. Bandyopadhyay, Macroscopic Fracture Behaviour: Correlation with Macroscopic Aspects of Deformation in Toughened Epoxies, *Toughened Plastics I: Science & Engineering*, C. Keith Riew and A.J. Kinloch, Eds., Advances in Chemistry Series 233, American Chemical Society, 1993, p 211–258
4. O. Frank and J. Lehmann, Determination of Various Deformation Processes in Impact-modified PMMA at Strain Rates up to 103 Per Minute, *Colloid Polym. Sci.*, 1986, **264**, p 473–481
5. R.W. Truss and G.A. Chadwick, The Tensile Deformation Behaviour of a Transparent ABS Polymer, *J. Mater. Sci.*, 1976, **11**, p 1385
6. R.K. Goldberg, G.D. Roberts, and A. Gilat, Incorporation of Mean Stress Effects into the Micromechanical Analysis of the High Strain Rate Response of Polymer Matrix Composites, *Compos. Part B*, 2003, **34**, p 151–165
7. C. Grein, H.-H. Kausch, and Ph. Béguelin, Characterisation of Toughened Polymers by LEFM Using an Experimental Determination of the Plastic Zone Correction, *Polym. Testing*, 2003, **22**, p 733–746
8. T. Vu-Khanh and Z. Yu, Mechanisms of Brittle-ductile Transition in Toughened Thermoplastics, *Theor. Appl. Fract. Mech.*, 1997, **26**, p 177–183
9. W. Jiang, D. Yu, and B. Jiang, Brittle-Ductile Transition of Particle Toughened Polymers: Influence of the Matrix Properties, *Polymer*, 2002, **45**, p 6427–6430
10. C. Fond and R. Schirrer, Dynamic Fracture Surface Energy Values and Branching Instabilities During Rapid Crack Propagation in Rubber Toughened PMMA, C. R. Acad. Sci. Paris, t. 329, Série II b, 2001, p 195–200
11. P.A. Tzika, M.C. Boyce, and D.M. Parks, Micromechanics of Deformation in Particle-toughened Polyamides, *J. Mech. Phys. Solids*, 2000, **48**, p 1893–1929
12. G.M. Kim and G.H. Michler, Micromechanical Deformation Processes in Toughened and Particle Filled Semicrystalline Polymers. Part 2: Model Representation for Micromechanical Deformation Processes, *Polymer*, 1998, **39**(22), p 5699–5703
13. S. Biwa, N. Ito, and N. Ohno, Elastic Properties of Rubber Particles in Toughened PMMA: Ultrasonic and Micromechanical Evaluation, *Mech. Mater.*, 2001, **33**, p 717–728
14. N. Murphy and A. Ivankovic, The Prediction of Dynamic Fracture Evolution in PMMA Using a Cohesive Zone Model, *Eng. Fract. Mech.*, 2005, **72**, p 861–875
15. X.F. Yao, W. Xu, M.Q. Xu, K. Arakawa, T. Mada, and K. Takahashi, Experimental Study of Dynamic Fracture Behavior of PMMA with Overlapping Offset-parallel Cracks, *Polym. Testing*, 2003, **22**, p 663–670
16. F. Zhou, J.-F. Molinari, and T. Shioya, A Rate-dependent Cohesive Model for Simulating Dynamic Crack Propagation in Brittle Materials, *Eng. Fract. Mech.*, 2005, **72**, p 1383–1410
17. D. Taylor, M. Merlo, R. Pegleya, and M.P. Cavatorta, The Effect of Stress Concentrations on the Fracture Strength of Olymethylmethacrylate, *Mater. Sci. Eng. A*, 2004, **382**, p 288–294
18. W. Loyens and G. Groeninckx, Deformation Mechanisms in Rubber Toughened Semicrystalline Polyethylene Terephthalate, *Polymer*, 2003, **44**, p 4929–4941
19. C.B. Bucknall, I. Partridge, and M.V. Ward, Rubber Toughening of Plastics, *J Mater. Sci.*, 1984, **19**, p 2064–2082
20. O. Julien, Ph. Begulin, I. Monnerie and H.-H. Kausch, Loading-rate Dependence of the Fracture Behaviour of Rubber-modified poly(methyl methacrylate), *Toughened Plastics II: Novel Approaches in Science & Engineering*, C. Keith Riew and A.J. Kinloch, Eds., Advances in Chemistry Series 252, American Chemical Society, 1996, p 233–252
21. A. Savadori, Methods of Measurements and Interpretation of Results, in *Rubber Toughened Engineering Plastics*, A.A. Collyar, Ed. Chapman & Hall, London, 1994, p 90–135
22. R.W. Truss and G.A. Chadwick, Tensile Behaviour of ABS Polymers, *J Mater. Sci.*, 1976, **11**, p 111–117
23. D. Broek, *Elementary Engineering Fracture Mechanics*. Martinus Nijhoff Publishers, Dordrecht, 1986
24. S. Gong, S. Bandyopadhyay, Mechanical Properties and Fracture Surface Morphologies in Unnotched Specimens of Rubber-PMMA Composites *J. Mater. Eng. Perform.*, 2007, doi: 10.1007/s11665-007-9042-2
25. D.R. Askeland and P.P. Phulé, *The Science and Engineering of Materials*, 4th ed., Brooks Cole Publishing, A Division of Thomson Learning, 2004
26. P.A. Lovell, J. McDonald, D.E.J. Saunders, M.N. Sherratt and R.J. Young, Multiple-phase Toughening-particle Morphology: Effects on the Properties of Rubber-toughened Poly(methyl methacrylate), *Toughened Plastics I: Science and Engineering*, C. Keith Riew and A.J. Kinloch, Eds., Advance in Chemistry Series 233, American Chemical Society, 1993, p 61–77
27. C.R. Brooks and A. Choudhury, *Failure Analysis of Engineering Materials*. McGraw-Hill Companies, New York, 2002